2014

APPLICATION OF HIGH-INTENSITY FOCUSED ULTRASOUND TO THE STUDY OF MILD TRAUMATIC BRAIN INJURY

Joseph T. McCabe
Uniformed Services University of the Health Sciences, USUHS, The Center for Neuroscience and Regenerative Medicine, Joseph.McCabe@usuhs.edu

Chantal Moratz
USUHS, The Center for Neuroscience and Regenerative Medicine

Yunbo Liu
Center for Devices and Radiological Health, Food and Drug Administration

Ellen Burton
The Center for Neuroscience and Regenerative Medicine, USUHS

Amy Morgan
The Center for Neuroscience and Regenerative Medicine, USUHS

See next page for additional authors

Authors
Joseph T. McCabe, Chantal Moratz, Yunbo Liu, Ellen Burton, Amy Morgan, Craig Budinich, Bennell Lowe, John Rosenberger, HuaZhen Chen, Jiong Liu, and Matthew Myers

Ultrasound in Med. & Biol., Vol. 40, No. 5, pp. 965–978, 2014
Published by Elsevier Inc. on behalf of World Federation for Ultrasound in Medicine & Biology
Printed in the USA. All rights reserved
0301-5629/$ - see front matter

http://dx.doi.org/10.1016/j.ultrasmedbio.2013.11.023

Ultrasound in Medicine & Biology, Volume 40, Issue 5, May 2014, Pages 965-978

● *Original Contribution*

APPLICATION OF HIGH-INTENSITY FOCUSED ULTRASOUND TO THE STUDY OF MILD TRAUMATIC BRAIN INJURY

JOSEPH T. MCCABE,*†‡ CHANTAL MORATZ,†‡§ YUNBO LIU,‖ ELLEN BURTON,‡§ AMY MORGAN,‡§ CRAIG BUDINICH,† DENNELL LOWE,* JOHN ROSENBERGER,* HUAZHEN CHEN,* JIONG LIU,* and MATTHEW MYERS‖

*Department of Anatomy, Physiology and Genetics, Uniformed Services University of the Health Sciences (USUHS), Bethesda, Maryland, USA; †Graduate Program in Neuroscience, USUHS, Bethesda, Maryland, USA; ‡The Center for Neuroscience and Regenerative Medicine, USUHS, Bethesda, Maryland, USA; §Department of Medicine, USUHS, Bethesda, Maryland, USA; and ‖Center for Devices and Radiological Health, Food and Drug Administration, White Oak, Maryland, USA

(*Received* 19 *June* 2013; *revised* 13 *November* 2013; *in final form* 16 *November* 2013)

Abstract—Though intrinsically of much higher frequency than open-field blast overpressures, high-intensity focused ultrasound (HIFU) pulse trains can be frequency modulated to produce a radiation pressure having a similar form. In this study, 1.5-MHz HIFU pulse trains of 1-ms duration were applied to intact skulls of mice *in vivo* and resulted in blood-brain barrier disruption and immune responses (astrocyte reactivity and microglial activation). Analyses of variance indicated that 24 h after HIFU exposure, staining density for glial fibrillary acidic protein was elevated in the parietal and temporal regions of the cerebral cortex, corpus callosum and hippocampus, and staining density for the microglial marker, ionized calcium binding adaptor molecule, was elevated 2 and 24 h after exposure in the corpus callosum and hippocampus (all statistical test results, $p < 0.05$). HIFU shows promise for the study of some bio-effect aspects of blast-related, non-impact mild traumatic brain injuries in animals. (E-mail: Joseph.McCabe@usuhs.edu) Published by Elsevier Inc. on behalf of World Federation for Ultrasound in Medicine & Biology.

Key Words: **Animal models, Blast injury, Blood–brain barrier, Mouse, High-intensity focused ultrasound, Traumatic brain injury.**

INTRODUCTION

Civilian and military personnel exposure to violent explosions, often from improvised explosive devices (IEDs), has burgeoned with recent world events (Aschkenasy-Steuer et al. 2005; Cernak et al. 1999; DuBose et al. 2011). In military populations, a RAND report (Tanielian and Jaycox 2008) estimated that as many as 20% (~320,000) of military personnel experienced some form of traumatic brain injury (TBI). In terms of severe TBI, a recent survey found that the majority are related to explosives (Wojcik et al. 2010), and severe blast-related traumatic brain injuries are a component of multiple injuries; a significant challenge to polytrauma care specialists (Aschkenasy-Steuer et al. 2005; DuBose et al. 2011) and a hardship to the patient and family during rehabilitation and lifestyle adjustments (Bazarian et al. 2009; Sayer et al. 2008).

Milder forms of TBI are also a significant medical, social and economic challenge. Mild TBIs (mTBIs), in fact, constitute the majority of cases of blast-related exposures. Although nearly all individuals who sustain mTBIs eventually improve (Brown et al. 2011), residual cases persist and are likewise an ordeal for patient and caretakers and a challenge for neuropathological and imaging diagnosis, therapies, surgical reconstruction and home life adjustments (Silver et al. 2009; Tanielian and Jaycox 2008). In a sense, milder TBI has been enigmatic. The individual may have no other significant injuries, complaints may have a slower onset that is not evident as an acute manifestation and symptoms overlap and are concomitant with post-traumatic stress disorder (PTSD) diagnoses. Because of the lack of easily identifiable criteria for the critical factors related to pathophysiology, mild blast-related TBI is a significant challenge for pre-clinical researchers as well. Basic research

Address correspondence to: Joseph T. McCabe, Department of Anatomy, Physiology & Genetics, The Center for Neuroscience & Regenerative Medicine, Uniformed Services University of the Health Sciences, 4301 Jones Bridge Road, Bethesda, MD 20814-4799, USA. E-mail: Joseph.McCabe@usuhs.edu

Conflicts of Interest: The authors have indicated that they have no conflicts of interest regarding the content of this article.

is essential for the development of a better understanding of the mechanisms of milder TBI and how best to discover therapies.

Of particular interest in blast TBI is the high overpressure generated by the detonation process. This intense, entirely compressive phase of the wave is a few milliseconds in duration. Blast overpressure has been implicated in "primary" blast injury (Chen and Huang 2011; Elder and Cristian 2009; Taber et al. 2006), though the mechanisms are not well understood. There is a need for models to generate blast-like overpressures in animals, so that injury mechanisms can be studied and neurotherapeutics investigated.

One method for generating overpressures representative of actual explosions is the use of gas-driven overpressure shock tubes (Bauman et al. 2009; Chavko et al. 2008; Desmoulin and Dionne 2009; Gorbunov et al. 2008; Long et al. 2009; Risling and Davidsson 2012; Sundaramurthy et al. 2012; Svetlov et al. 2010). Although blast shock tube models are state-of-the-art for investigation of the mechanisms related to blast-induced TBI, there are some limitations to their use. First, with the exception of placing the animal inside a flak jacket or other protective enclosure, the entire body is exposed to the overpressure wave. Second, with the exception of peak pressure, the waveform is relatively impervious to modulation and dependent on tube dimensions and animal placement. Third, there are important considerations with respect to the scale difference between human exposures and animal models (Bass et al. 2011). A free-field blast wave may operate at ~30-cm wavelength and have significant variation within the human body, including within the head region. In contrast, the smaller overall size of rodents produces an animal model with an essentially uniform stress field incident on the subject.

An alternative approach for studying the biological effects of exposure to high pressures involves the use of high-intensity focused ultrasound (HIFU). HIFU has been applied to the brain in such applications as tumor ablation, clot dissolution and drug delivery across the blood-brain barrier. These brain applications, and other HIFU procedures, are reviewed by ter Haar (2007). Tumor ablation is accomplished through intense heating arising from absorption of the HIFU beam. In clot dissolution and ultrasound-enhanced drug delivery, cavitation is typically induced through the introduction of ultrasound contrast agents (Park et al. 2012; Samiotaki et al. 2012).

In the present application of HIFU, neither the thermal nor the cavitational mechanism is operational. A similar and related application is acoustic neuromodulation, where, as part of treatment for a variety of neurologic disorders, ultrasound waves are used to control neuronal activity without producing heat or cavitation (Gavrilov et al. 1996; Min et al. 2011; Tufail et al. 2010; Tyler et al. 2008). In contrast to the therapeutic objective of acoustic neuromodulation, the intention of the present work was to induce mild injury in the brain. However, as with neuromodulation, heating is not desirable when trying to reproduce the bio-effects of blasts because, with the exception of extremely powerful explosions, the duration is too short for significant heating to occur in actual blasts. Cavitation is likewise absent during the overpressure (compression) phase of a blast wave. The goal in our HIFU application was to generate force on brain tissue that changes in magnitude but not direction during the duration of the wave, as in a blast exposure. Our hypothesis was that the blast-like temporal variations in this force, along with the spatial variations naturally occurring in a HIFU beam, would produce some of the biological effects occurring during blast exposure. The HIFU model was constructed in the following manner.

The HIFU overpressure simulator produces a megahertz-frequency carrier wave whose amplitude is modulated so that the amplitude envelope possesses a shape similar to that of the overpressure of a blast wave. Although some difference will always exist between the blast overpressure and the HIFU envelope because of the negative swings of the HIFU pulses, the negative portions are significantly lower in amplitude than the positive segments. In terms of root mean square (RMS) pressure or radiation force, which does not change sign during the duration of the wave, the shape correspondence between the actual blast and HIFU-simulated overpressures is more exact. With respect to absolute pressure levels, the pressure amplitude or RMS pressure of the HIFU-simulated wave is typically higher than that of the blast overpressure, while the radiation pressure is considerably lower. It is unclear which bio-effects are related to which characteristics of the blast (or simulated blast) field; this issue is explored in the final section. To the extent that brain tissues respond to radiation force, or shear stresses arising from spatial variations in this force, the HIFU blast simulator is promising for studying mild traumatic brain injury. The utility of the HIFU model is evaluated by assessing the response of the mouse brain to the HIFU-simulated overpressures, as described below, after some of the features motivating the HIFU approach are presented.

The HIFU model possesses several practical attributes that are desirable for studying brain injury. For one, the focusing feature of HIFU limits the complexity of system response to the stress field. By sonicating only a portion of the brain with the narrow (a few millimeters in water) beam, we do not have as complex an endocrine/immune response and trauma as is seen in a whole-body blast. This allows for a more controlled study of bio-effects, as well as a more systematic investigation

of the efficacy of potential neurotherapeutics. With some animal models (probably rat-sized or larger), the unsonicated side of the brain can also serve as control for the exposed half. The intensity and shape (as a function of time) of a HIFU-simulated overpressure can be varied in a highly controlled and reproducible manner by adjusting the function generator driving the HIFU transducer. For research throughput, because there is a requirement for a short state of anesthesia followed by immediate blast exposure, HIFU is an advantageous model for blast-induced brain injury. Finally, HIFU uses no explosives or pressurized gases that may cause physical or auditory damage that could arise from the use of a shock tube.

To evaluate the HIFU overpressure simulator in a mouse model, laboratory mice were exposed to the amplitude-modulated HIFU pulse trains, and multiple assessments of mild traumatic brain injury were made. First, examinations were made for any infiltration of dye into the brain parenchyma after blast exposure. Alterations in endothelial cells were also evaluated by examining antibody adherence within cerebral vascular walls. Immune response was identified by staining for signs of astrocyte and microglial activation. Additionally, as the HIFU model was designed to study mild traumatic brain injury, tests of moderate to severe brain injury were performed. These include staining for neuronal death and histologic examination for morphologic changes. The various measures of mTBI in the mouse model are described in greater detail in the next section.

METHODS

HIFU apparatus

Figure 1 is a schematic representation of the HIFU apparatus. A spherical transducer (Model MX-111, UTX, Holmes, NY, USA) of 1.5-MHz frequency having a diameter of 10 cm and a focal length of 15 cm was driven by two tandemly arranged waveform generators (Models 33220 A [20 MHz] and 33250 A [80 MHz] Function/Arbitrary waveform generators, Agilent, Santa Clara, CA, USA) and a 150-W broadband amplifier (Model 150 A100 B [10 kHz, 100 MHz]. Amplifier Research, Souderton, PA, USA). The first waveform generator produced a driving voltage in the form of a train of sinusoidal waves at the 1.5-MHz resonant frequency of the transducer. The second waveform generator modulated the amplitudes of the sinusoids so that the envelope connecting the maximum pressures of the sine waves had the desired shape of a blast overpressure. We emphasize that the envelope (and, as will be seen subsequently, the RMS pressure and radiation pressure) possesses the form of a blast overpressure, whereas the individual, high-frequency waves within the envelope do not. The magnitude of the driving voltage was between 100 and

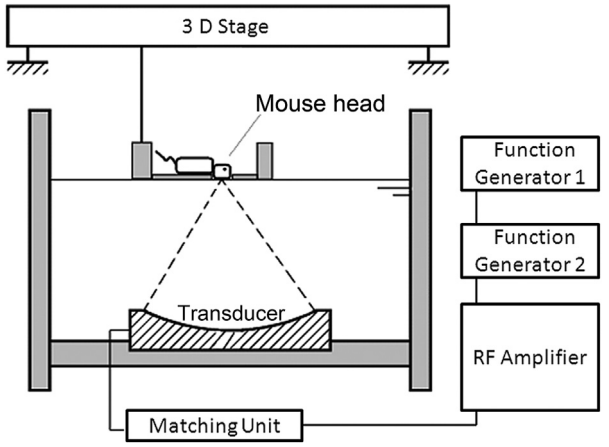

Fig. 1. Schematic of the components of the high-intensity focused ultrasound apparatus. The two in-tandem waveform generators provide input signal to a radiofrequency (RF) amplifier to emit a 1.5-MHz wave. The impedance matching unit delivers the signal to the high-intensity focused ultrasound transducer, which emits the wave with a focal point ~15 cm from the transducer. A hollow tray holds the anesthetized animal in a supine position. A hole in the tray is covered with cellophane, allowing the wave to pass through to the mouse's head.

400 mV, and the duration of the sinusoidal wave train was roughly 1 ms, the approximate duration of a blast overpressure. Although the pulses were sinusoidal at the transducer, they developed into more of a sawtooth (shock wave) form at the target because of non-linear propagation in the water. The pressure field generated by the transducer is presented in the Results.

Measurement of pressure field generated by HIFU system

A ceramic needle hydrophone (HNA400, Onda, Sunnyvale, CA, USA) was used to measure the temporal and spatial pressure characteristics generated by the HIFU transducer. The transducer was placed in a water tank horizontally, and the hydrophone was controlled by an acoustic measurement system (Sonora Medical System, Longmont, CO, USA) that systematically moved the hydrophone through the ultrasound field emitted by the transducer. Pressure values were obtained in millivolts and converted to megapascals by dividing by the hydrophone sensitivity (provided by Onda). To assess the impact of the skull interface on HIFU transmission, both mouse and rat parietal (skull) bones were placed a distance of 5 mm in front of the hydrophone, in a water tank filled with degassed water. Pressure measurements were repeated with and without the bone interface, as a means of estimating acoustic loss and beam spreading.

Animals

C57/Bl6 male mice (7–8 wk of age) were obtained from Jackson Labs (Bar Harbor, ME, USA), and housed

in groups of five mice per cage in the USUHS Department of Laboratory Animal Medicine. All studies were approved by the USUHS Institutional Animal Care and Use Committee. Animals were maintained on a 12:12-h light:dark cycle and had *ad libitum* access to food and water. Animals were housed at least 1 wk in the USUHS animal facility before use.

HIFU exposure procedure

At the time of HIFU exposure, mice were anesthetized with 5% isoflurane for 2–3 min and then maintained on 2% isoflurane for the remainder of the procedure. After loss of consciousness, fur was removed from the dorsal scalp region with a depilatory agent (Nair; Church & Dwight, Princeton, NJ, USA) and the area wiped clean with water. The scalp was then coated with hydrogel (Aquasonic 100 US Transmission Gel, REF01-02, Parks Labs, Fairfield, NJ, USA) and the mouse was placed in a supine position on top of a small plastic tray. The floor of the tray had a 2-cm opening in the base that was covered with a thin layer of plastic. The coated scalp was placed on the plastic film and the device lowered to the water surface to direct the wave to the right cerebral hemisphere. Animals that were assigned to the HIFU exposure condition were placed on the platform and were exposed to a 1-ms pulse, and the signal generator was adjusted to control wave amplitude. As described below, a 400-mV setting was used for *in vivo* experiments. Sham animals were placed on the platform but were not exposed to HIFU.

After exposure to HIFU (see below), animals regained consciousness and were returned to their home cages and observed for 2 h. After the observation period, the animals were either sacrificed to obtain samples for the 2-h time point or returned to the animal facility where they were later terminated to obtain the 24-h time point. The animals received anesthesia by the administration of ketamine and xylazine (80 and 10 mg/kg body weight, respectively) before they were sacrificed. In some cases, the brain was removed from the calvarium and used to evaluate blood-brain barrier status, while other mice received perfusion fixation for histopathology.

Brain tissue processing

To evaluate the effects of HIFU exposure on the cerebral vasculature, individual rodents were anesthetized with ketamine and xylazine (80 and 10 mg/kg body weight, respectively) and placed in a Plexiglas animal restraint apparatus to permit infusion of 100 μL of a 1% Evans blue dye solution (Catalog No. 151108, ICN Biochemicals, Aurora, OH, USA) into the tail vein 30 min before HIFU or sham (no HIFU exposure) treatment. Evans blue binds to albumin, allowing visualization of plasma protein extravasation with disruption of the blood-brain barrier. To evaluate Evans blue staining, 2 after HIFU exposure (see below), the animals were anesthetized and the brain was removed from the calvarium for photographic recording of Evans blue on the cerebral surface. Brains were examined by placing them on an inverted Zeiss microscope and the exposing the surface to 550-nm excitation (573-nm emission range). Because of the presence of the dye, fluorescence permitted visualization of cerebral vessels.

To evaluate neuropathological changes, animals were anesthetized 2 or 24 h after HIFU exposure for histochemical processing. When unresponsive, the thoracic cavity was exposed and animals were transcardially perfused with normal saline until the perfusate was cleared of blood, and then with 4% paraformaldehyde in phosphate-buffered saline (PBS). The brains were then removed from the calvarium and post-fixed in paraformaldehyde for 24 h, submerged in 20% sucrose in PBS for 24 h and placed in 30% sucrose-PBS. Frozen (30-μm-thick) coronal sections were obtained for hematoxylin and eosin (H&E) histology and for anti-IgG immunohistochemistry. For IgG staining, AffiniPure F(ab')2 fragment goat anti-mouse IgG (1:300 dilution, Catalog No. 115-006-072, Jackson ImmunoResearch Laboratories, West Grove, PA, USA) was incubated on sections. After incubation with rabbit anti-goat horseradish peroxidase IgG (KPL 14-13-06, KPL, Gaithersburg, MD, USA), sections were developed with the Vector SK4100 DAB kit (Vector Laboratories, Burlingame, CA, USA) to visualize IgG staining.

Additional sections were used for other purposes: to assess neuronal cell death using Fluoro-Jade B (AG310, EMD Millipore, Billerica, MA, USA) histochemistry; to assess astrocyte activation by immunohistochemical staining for glial fibrillary acidic protein (GFAP); and to evaluate microglial activation by staining for ionized calcium-binding adaptor molecule (Iba1). Fluoro-JadeB staining followed conventional protocols (Schmued and Hopkins 2000). Fixed, dried tissue sections were incubated in 1% NaOH/80% ethanol for 5 min, rinsed in ethanol and water, and placed in 0.66% potassium permanganate for 10 min. Sections were rinsed in water, and then placed in 0.0001% Fluoro-Jade B/0.1% acetic acid for 10 min, and then rinsed again in water, dried, cleared with xylenes, and coverslipped. For GFAP immunohistochemistry, the Vector M.O.M. Immunodetection Kit was used to reduce endogenous IgG binding. After blocking, the brain sections were incubated (overnight at 4°C) with the GFAP Ab-1 monoclonal antibody (No. MS-280-P0, 1:500, Thermo Scientific, Pittsburgh, PA, USA) in PBS plus 0.2% Triton. A biotin-conjugated goat anti-mouse IgG1 was used to detect the primary antibody (1:500, Jackson ImmunoResearch Laboratories). For Iba1 (also called allograft inflammatory

factor or microglia response factor 1) immunohistochemistry, sections were incubated in a 1:4000 dilution of Iba1 (No. 019-19741, Wako, Richmond, VA, USA) for 24 h. The primary antibody was detected after a 1-h incubation in a biotin-conjugated goat anti-rabbit IgG (1:250. Jackson ImmunoResearch Laboratories). For both GFAP and Iba1 immunohistochemistry, sections were further processed for diaminobenzidine histochemistry per vendor instructions (Vector Laboratories). Specifically, the sections were incubated with strepavidin horseradish peroxidase (Vector SA-5004, 1:2500) for 1 h and then developed with the Vector SK4100 kit. Sections were then coverslipped and examined using bright-field microscopy.

A digital image (129,600 pixels) was taken of each sub-region of interest in each section to measure staining intensity using the ImageJ software (National Institutes of Health) (Collins 2007). Specifically, optical density measures of staining intensity were assessed in the parietal cortex, corpus callosum, hippocampus and temporal lobe (including the temporal cortex and amygdala). In each brain region, five or six stained sections were selected (that were at comparable anatomic locations and identical magnification for each brain region) to evaluate staining across treatment groups. A set of matched sections were stained with an isotype control antibody to evaluate non-specific binding. Density analysis of antibody staining was used to assess the relative change in protein expression across samples. Staining intensity measures were obtained by setting the background threshold using the matched isotype control stained section. The image was then converted to a 16-bit image, and the analysis function was used to measure the density. Once the threshold was set, the imaging software (Image J) computed the density value. Staining intensity measures between experimental treatment groups were then evaluated with an analysis of variance (SigmaStat, Version 3.11, Systat Software, San Jose, CA, USA) and when differences were found (statistical significance of $p < 0.05$), the Bonferroni *t*-test was used to evaluate differences between groups. Preliminary evaluation indicated all data sets passed tests for normality and equal variance, with the exception of the data obtained from measures from the parietal cortex region for GFAP and the vessel density measures for Iba1. A natural logarithm transformation was performed on these data sets, which then met preliminary test criteria.

RESULTS

Characteristics of HIFU-simulated overpressure

Pressure measurements were obtained at the focus of the HIFU transducer, as well as other locations in the focal plane. Figure 2 illustrates the waveform at the focus when the waveform generator was set to 40, 100 and 400 mV and measured in water (*left traces*) or behind a mouse parietal bone (*right traces*). In the top two and middle two traces it can be seen that when the voltage was 40 or 100 mV, respectively, the positive portion of the high-frequency wave train was approximately equal to the negative portion. However, when the waveform generator was set to 400 mV (*bottom two traces*), the positive portion of the wave train was considerably stronger (~10 MPa max) than the negative portion (–2 MPa min). In Figure 3a, the pressure trace for an individual pulse of the pulse train is plotted, at a location near the focus and a time where the modulated amplitude is approximately 7 MPa. Steepening of the pulse, which is sinusoidal at the transducer surface, can be observed. A measure of the acoustic energy incident on the brain tissue as a function of time throughout the duration of the simulated overpressure can be obtained by computing the RMS pressure of the amplitude-modulated (AM) wave. The RMS pressure is given by

$$p_{\mathrm{RMS}}(t) = \left[\frac{1}{T}\int_{t}^{t+T} p^2(t')dt'\right]^{1/2}. \qquad (1)$$

where T is the period of the high-frequency pulse, roughly 0.6 μs. The RMS pressure for the AM pulse train, measured in water, is illustrated in Figure 3b. As noted in the previous section, the pulse of Figure 3a does not have a shocked, blast-like profile. Rather, a train of thousands of such pulses of properly modulated amplitude is concatenated to produce the blast-like profile of Figure 2 (*bottom trace*) and Figure 3b.

To estimate the modification of the simulated overpressure wave caused by the presence of the skull, pressure levels were made distal to mouse and rat skull samples. Plots of RMS pressure inside the mouse and rat skull samples, as well as in water, are provided in Figure 4a (water), 4b (mouse) and 4c (rat). Scales for the three figures are different, although all units are kilopascals (kPa). The maximum pressure inside the mouse skull is approximately 35% of the peak pressure in water alone, and the maximum pressure inside the rat skull is about 18% of the peak water value. In terms of beam width, the width corresponding to a 50% reduction in pressure is approximately 2 mm in water. The beam width in the presence of the mouse was approximately 2.5 mm. Spreading by the rat skull was more severe, and the rat skull distorted the HIFU beam into more of an ellipsoidal shape. The beam width, again determined from the dimension of the 50% pressure contour, was about 2.5 mm in one direction and 3.5 mm in the other.

In the Introduction, we noted that the bio-effects of blast overpressures are not due to heating or cavitation,

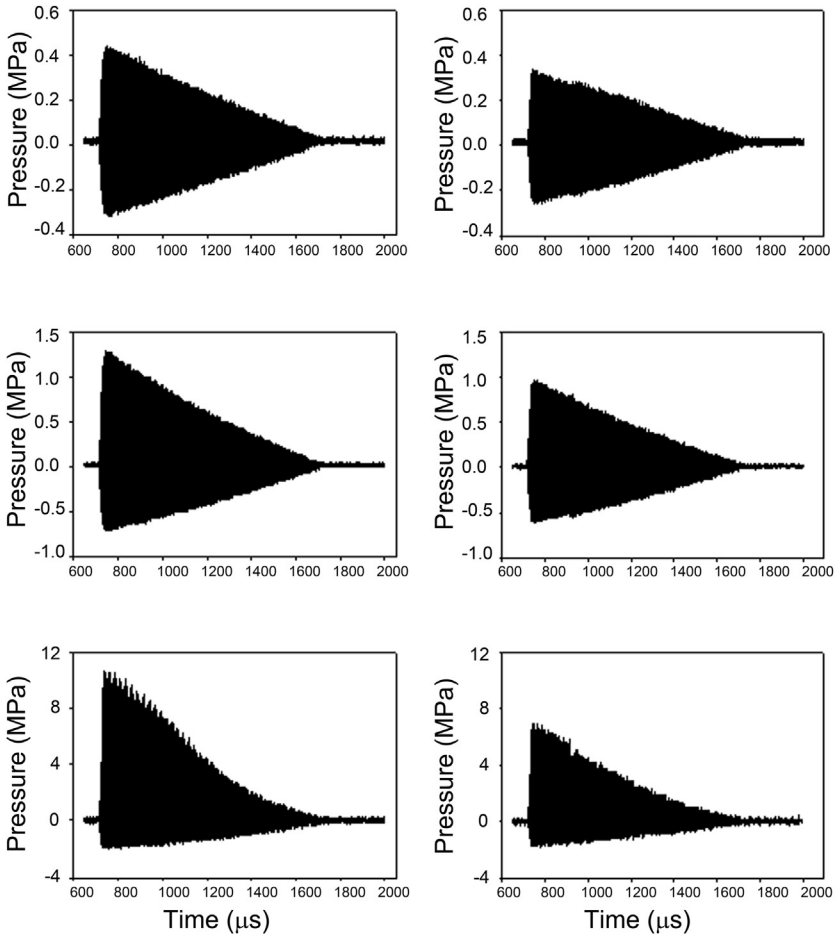

Fig. 2. Temporal profile of pressure waves in water (in MPa) at amplitude-modulated voltage settings of 40 (top traces), 100 (middle traces) and 400 mV (bottom traces). The duration of the amplitude-modulated wave trains shown was 1000 μs. Traces in the left column were obtained in water, and those in the right column were recorded inside the parietal bone from a mouse. With the 400-mV wave, the upper envelope of the wave mimics the almost instantaneous rise in pressure seen in a free-field blast, followed by an exponentially decaying tail. The lower envelope has a similar but inverted shape and is about one-third of the upper envelope in amplitude. Also evident is the attenuation in pressure as a result of the intervening bone, while the waveform is slightly altered.

and hence, it is desirable to eliminate these effects from the HIFU-simulated overpressure as well. Thermal effects can be estimated as follows. The temperature rise in the brain can be estimated by solving the heat equation (Nyborg 1988)

$$\frac{\partial T}{\partial t} = \kappa \nabla^2 T + \frac{q}{\rho_0 c_p} \tag{2a}$$

where T is the temperature rise in the brain, κ is the thermal diffusivity of brain tissue and c_p is the specific heat. For linear acoustic propagation, the heat source is given by $q = 2\alpha I$, where α is the acoustic attenuation and I the time-averaged intensity. In the present case, harmonic generation occurs as a result of non-linear propagation effects, and the heat source is a sum of the heat sources due to absorption of the individual propagation modes (Myers and Soneson 2009):

$$q = \sum 2\alpha_n I_n \tag{2b}$$

Here, α_n is the value of the acoustic attenuation at the frequency of the nth harmonic, and I_n is the intensity of the nth harmonic. The intensities I_n can be related to the amplitudes a_n of the pressure harmonics using the standard plane wave approximation:

$$I_n = \frac{a_n^2}{\rho_0 c_0} \tag{3}$$

An upper bound for the temperature rise can be obtained by ignoring cooling caused by diffusion and integrating the source term in (2) to obtain

$$T = \frac{q}{\rho_0 c_p} \Delta t, \quad (4)$$

where Δt is the duration of the overpressure (roughly 1 ms). The modal amplitudes a_n required for q were obtained by decomposing the measured pressure trace in Figure 3a into a Fourier series. The frequency dependence of the attenuation was assumed to have the form $\alpha = af^b$ (Duck 1990), where the values $a = 0.067$ cm^{-1} $\text{MHz}^{-\text{b}}$ and $b = 1.3$, typical for the human brain (Duck 1990), were assumed. The frequency of the nth mode is given by nf_0, where f_0 is the transducer resonant frequency, 1.5 MHz. Using typical values of 1000 kg/m^3 for tissue density, 1500 m/s for the speed of sound and a heat capacity of $c_\text{p} = 4000$ J/(kg K) for brain (International Commission on Radiation Units and Measurements [ICRU] 1998), it is estimated there is a temperature rise of approximately 0.07°C for a 0.001-s overpressure. This amount of temperature rise is well below the threshold for any thermal bio-effects.

The absence of cavitation must also be verified, because even for blast overpressures, cavitation can occur during the rebound phase, especially if any gas bubbles are present. Gateau et al. (2011) found that for 660-kHz pulses, formation of gas bubbles in the sheep brain did not occur when the peak negative pressure was weaker than –12.7 MPa. Fry et al. (1995) found the cavitation threshold in dog brain tissue to be around –3.5 MPa for a 1-MHz pulse. The 1.5-MHz pulses used in our studies would likely have thresholds that were more negative than these values. Given that the worst-case negative pressure in Figure 2 was approximately –1.7 MPa, and the average peak negative pressure for the wave train was less than –1 MPa, it is unlikely that the negative pressures occurring during the HIFU exposures produced cavitation. This conclusion was confirmed by examination of harvested mice brains, in which the pitting characteristic of cavitation damage was not observed.

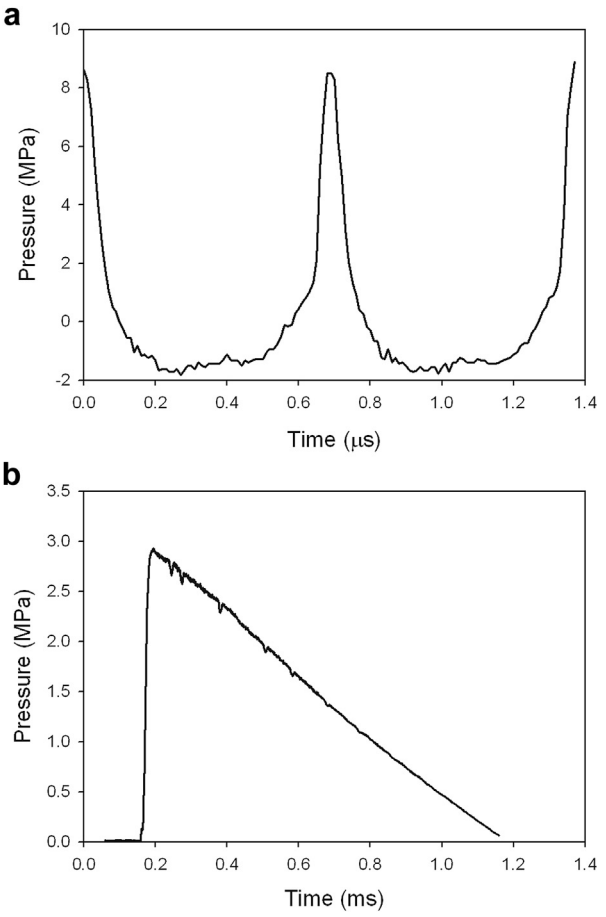

Fig. 3. Measurement of high-intensity focused ultrasound-generated pressure in water. (a) The rise time to maximal pressure for a single wave is approximately 3.5 μs. The pulse has steepened considerably from the sinusoidal form it possessed when radiated by the transducer. (b) To evaluate the average pressure change as a function of time, the root mean square average for each high-frequency pulse in the train for the amplitude-modulated wave was integrated over time (see eqn [1] in text), providing an estimate of intensity of a 400-mV wave.

Blood–brain barrier function

Compared with the pink appearance of the fresh brain samples from mice that received no injection (data not shown), animals that had received a tail vein injection of 2% Evans blue had a blue coloration observable over the entire neuraxis. The dye distribution in sham-treated animals (Fig. 5a) was considerably lighter than what was observed on the brain surfaces of mice that had been exposed to HIFU (Fig. 5b). *Ex vivo* imaging of the brain of HIFU-exposed and sham-treated animals was visualized by low-power fluorescence microscopy. The Evans blue dye was observed within the lumen of superficial cerebral vessels of sham-treated (Fig. 5c) and HIFU-exposed samples (Fig. 5d). However, the appearance of the dye differed after HIFU exposure. There was evidence of Evans blue dye accumulation within cerebral vessels from HIFU-exposed animals (Fig. 5c) that was not observed in sham-treated rodents (Fig. 5d). Additionally, perhaps consistent with the diffuse dye distribution observed on the brain surface (Fig. 5b), there was evidence of dye seepage into the brain parenchyma (Fig. 5d).

Immunoglobulin G staining was performed to determine if HIFU exposure resulted in the appearance of immunoglobulin in the brain parenchyma. In Figure 6, sections of cerebral cortex tissue from an animal that received sham treatment (*left*) or HIFU exposure (*right*) indicate there was an increase in IgG accumulation in cerebral vessels 2 h after HIFU exposure. However, there was no evidence of infiltration of IgG or IgM into brain parenchyma (data not shown).

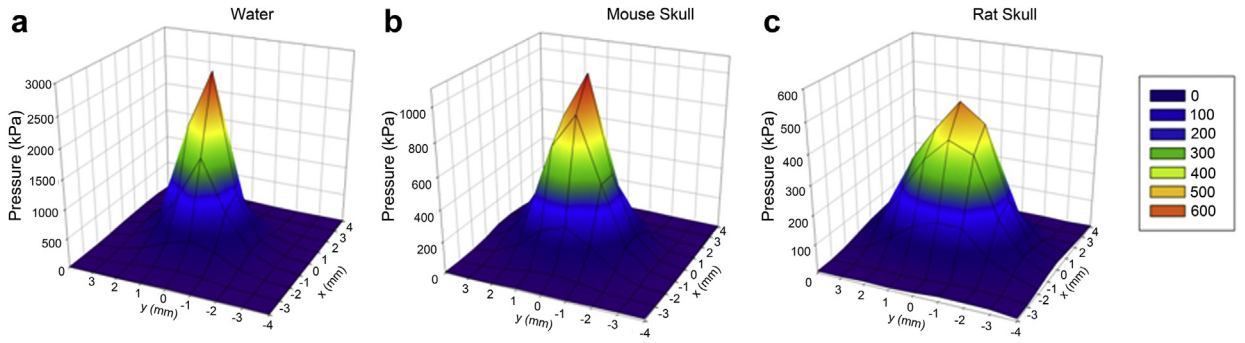

Fig. 4. Three-dimensional plots of pressure measurements of the high-intensity focused ultrasound waveform generated at the focal point. The colorized cone surfaces of the graphs illustrate changes in pressure as a function of distance from the beam axis. Relative to pressure measurements in water (a), there was approximately 65% and 82% attenuation of pressure in mouse and rat skulls (b, c).

Alteration in immunostaining for GFAP and Iba1 was used to assess histopathological response to HIFU exposure. GFAP immunostaining indicated changes in the density of astrocyte GFAP after a single exposure (Fig. 7). Analysis of variance of staining density measures for GFAP indicated that by 2 h after HIFU exposure, there was no change in GFAP staining density in the cerebral cortex, corpus callosum or hippocampus, but a

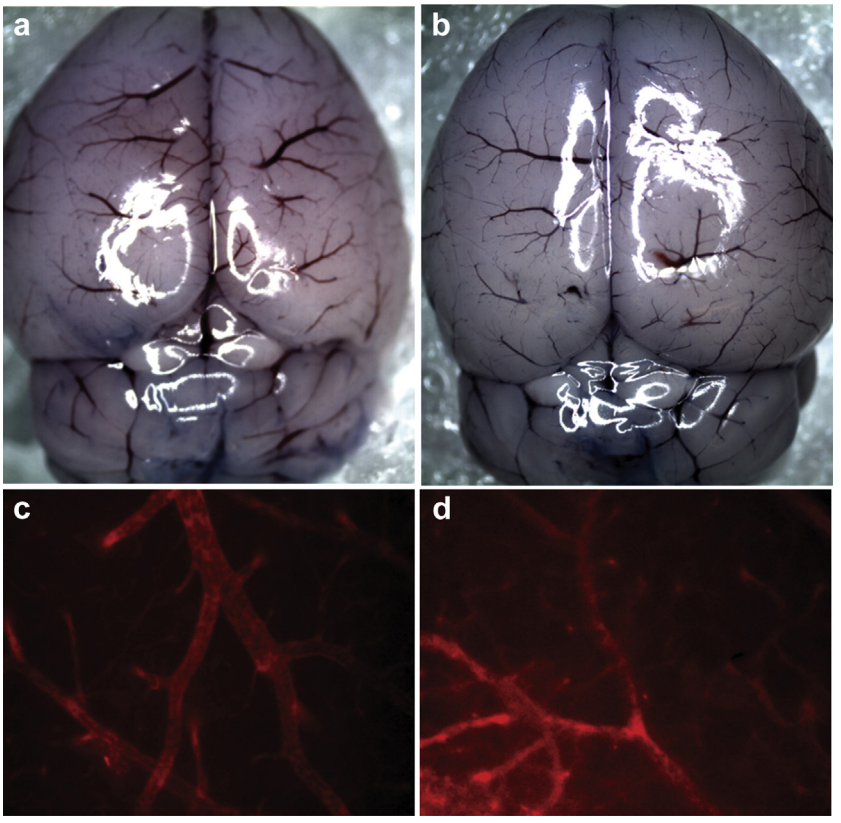

Fig. 5. *Ex vivo* photographs from animals that received a tail vein injection of a 2% Evans blue solution 30 min before sham treatment (a) or were subjected to a single 1-ms high-intensity focused ultrasound (HIFU) exposure (b). For sham treatment, animals were anesthetized and placed on the HIFU unit, but not exposed to HIFU. HIFU exposure resulted in greater diffuse coloring of dye on the surface of the entire neuraxis 2 h after HIFU exposure (b). At 540 nm excitation, Evans blue dye fluoresced cerebral vessels. Evans blue accumulated within the lumen of vessels after the sham treatment (c) or HIFU exposure (d), but there was evidence of adherence of dye within the lumen of vessels and dye seepage into the brain parenchyma (d) 2 h after HIFU treatment.

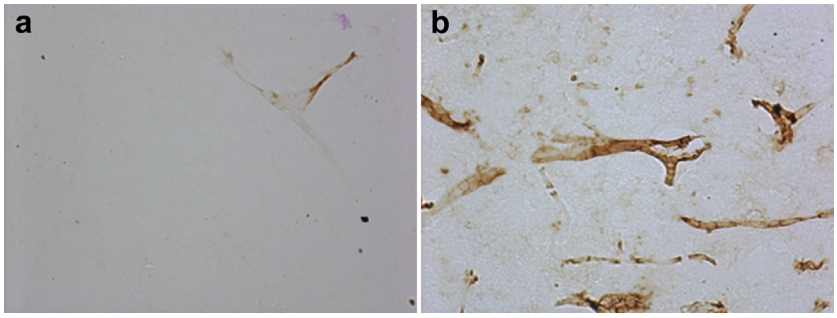

Fig. 6. Immunoglobulin G staining in cerebral vessels after exposure to high-intensity focused ultrasound (HIFU). Animals were exposed to a single 1-ms HIFU wave. Two hours after exposure, IgG staining was not prevalent in the brain sections obtained from sham-treated mice (a). However, IgG staining was observed in brain sections from HIFU-treated animals in close association with cerebral vessel inner walls (b).

significant increase was seen in the temporal lobe compared with staining of sham controls ($F_{2,17} = 8.06$, $p = 0.003$, Bonferroni *t*-test, $p = 0.011$ compared with sham treatment). However, by 24 h after exposure, GFAP staining density was increased in all of these brain regions (cerebral cortex: $F_{2,18} = 5.55$, $p = 0.013$, Bonferroni *t*-test, $p = 0.012$ compared with sham treatment; corpus callosum: $F_{2,16} = 21.32$, $p < 0.001$, Bonferroni *t*-test, $p < 0.001$ compared with sham group and $p < 0.001$ compared with 24-h group; hippocampus: $F_{2,18} = 13.82$, $p < 0.001$, Bonferroni *t*-tests, $p < 0.001$ compared with sham group and $p = 0.008$ compared with 2-h group; temporal lobe: $F_{2,17} = 8.06$, $p = 0.003$, Bonferroni *t*-test, $p = 0.008$).

Immunostaining for Iba1 (Fig. 8a) suggested staining density was elevated as soon as 2 h after exposure, and continued to be elevated 24 h after exposure. Related to observed changes in the blood-brain barrier, perivascular microglia were also examined around vessels in the hippocampus. Density of Iba1 immunostaining appeared to be elevated in these cells (Fig. 8a, indicated by *arrows*). This was also the case in the corpus callosum, parietal cerebral cortex and temporal region (data not shown). Staining density measures confirmed visual observations. At 2 or 24 h after HIFU exposure (Fig. 8b), Iba1 staining intensity was significantly greater in the corpus callosum ($F_{2,13} = 14.69$, $p < 0.001$, Bonferroni *t*-tests, 2 h vs. sham $p = 0.007$, 24 h vs. sham $p < 0.001$), the hippocampus ($F_{2,12} = 8.25$, $p = 0.006$, Bonferroni *t*-tests, 2 h vs. sham $p = 0.006$, 24 h vs. sham not significantly different $p = 0.103$), the vessels within the hippocampus ($F_{2,11} = 6.08$, $p = 0.017$, Bonferroni *t*-tests, 2 h vs. sham $p = 0.016$, 24 h vs. sham not significantly different $p = 0.573$) and in the parietal region of the cerebral cortex ($F_{2,12} = 5.063$, $p = 0.025$, Bonferroni *t*-tests, 2 h vs. sham $p = 0.040$, 24 h vs. sham $p < 0.048$) and temporal lobe ($F_{2,12} = 10.74$, $p < 0.001$, Bonferroni *t*-tests, 2 h vs. sham $p = 0.003$, 24 h vs. sham $p < 0.035$).

Gross injury indications after HIFU exposure

Twenty-four hours after HIFU exposure, there was no evidence of injury or hemorrhage on the surface of the cerebrum. In addition, H&E staining indicated no evidence of neuropathological changes, microhemorrhage or cavitation, and there were no Fluoro-JadeC-positive neuron profiles, indicative of neuron cell death.

Behavioral effects of HIFU exposure

At a 1-ms, 400-mV setting (Fig. 2, bottom trace), behavioral and physical examination of mice 24 h after HIFU exposure suggested there were no significant neurologic impairments. During a 2-h post-exposure observation period and observation 24 h after exposure, there was no evidence of lethargy, impaired nesting behavior, anomalous response to cage movement or handling by the investigator, abnormal gait, head tilting, differences in weight change overnight, grooming impairment (ruffled coat) or malaise (sunken eyes, squinting).

DISCUSSION

Several measures suggested that a single 1-ms HIFU exposure had a significant impact on some features of the neurovascular unit (Abbott et al. 2006; Hawkins and Davis 2005), and that HIFU exposure may serve as a mTBI model for understanding central nervous system hazards from low energetic blasts. Evans blue staining within the brain parenchyma suggested that HIFU exposure caused impairment of the blood-brain barrier. Furthermore, accumulation of Evans blue dye on the luminal surface of the vascular endothelium suggested exposure augmented the adherence of serum albumin (and, perhaps, other less abundant serum proteins). Finally, immunostaining for IgG accumulation in cerebral vessels suggested an alteration of cell surface phospholipid composition or cell surface protein expression by the endothelium. Changes in the endothelium luminal

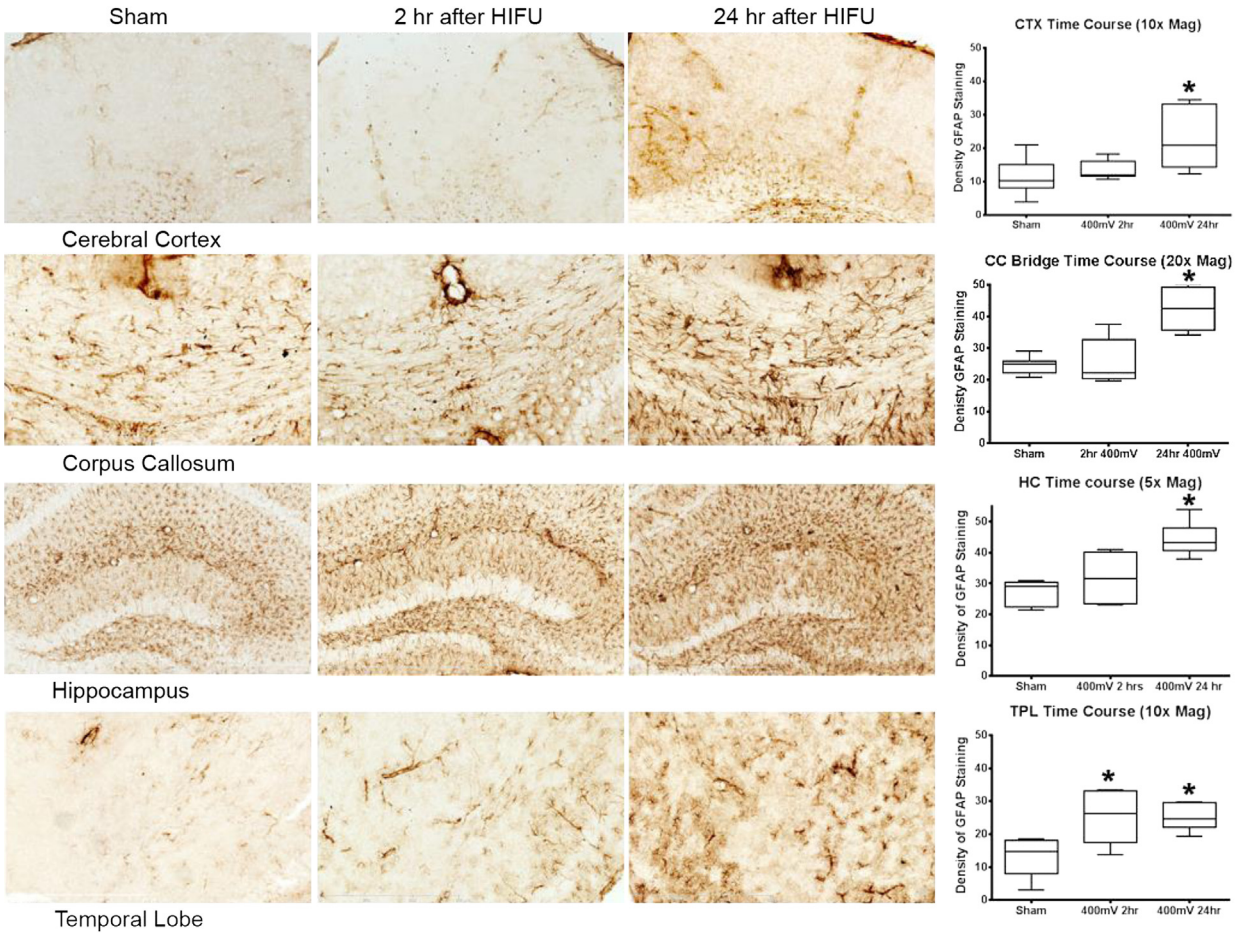

Fig. 7. Immunocytochemical staining for GFAP in sham animals, 2 and 24 h after exposure to HIFU. GFAP immunoreactivity was elevated slightly by 2 h after HIFU exposure (middle micrograph) and further enhanced by 24 h after HIFU exposure (rightmost micrograph). The plots to the right summarize the density of GFAP staining intensity for each treatment group. Box-and-whisker plots depict group medians (bars inside boxes) and 75th and 25th percentiles (upper and lower extents of the boxes), and the whiskers depict the 95th and 5th percentile estimations. Analysis of variance indicated there were significant changes in optical density for staining for GFAP after HIFU exposure (indicated by *asterisks*). By 2 h after exposure, compared with levels measured in sham-treated mice, the level of GFAP staining was significantly greater in the temporal lobe (*post hoc* Bonferroni *t*-test: $p = 0.011$). By 24 h after HIFU exposure, staining intensity for GFAP was significantly higher than levels in sham-treated mice in the cerebral (parietal) cortex ($p = 0.012$) and temporal lobe ($p = 0.008$) and significantly greater in the corpus callosum ($p < 0.001$ vs. sham group, $p < 0.001$ vs. 2-h group) and hippocampus ($p < 0.001$ vs. sham group, $p = 0.008$ vs. 2-h group) than both levels in sham-treated mice and levels measured 2 h after HIFU exposure. GFAP = glial fibrillary acidic protein, HIFU = high-intensity focused ultrasound, CTX = dorsolateral parietal region of the cerebral cortex, CC = corpus callosum, HC = hippocampus, TPL = temporal lobe of the cerebral cortex.

surface are a well-characterized phenomenon of vascular cell activation and injury (Kulik et al. 2009; Rao and Pendurthi 2012; Rosenberg 2012). The fact that no change in infiltration was seen with IgG or IgM, however, suggests that although there was perturbation of the endothelium, there was no evidence that under these conditions, HIFU exposure resulted in a shearing injury or a significant breach of the blood-brain barrier that permitted the infiltration of macromolecules in the range of ~150 kDa.

In addition to blood-brain barrier disruption, mTBI is characterized by astrocyte activation. In their study of traumatic brain injury induced by controlled cortical impact, Myer et al. (2006) concluded that reactive astrocytes play essential protective roles, by preserving neural tissue and restricting inflammation after moderate brain injury. In the present study, a single HIFU exposure was sufficient to elicit an elevation in GFAP immunostaining in astrocytes, a characteristic neuro-immune response to blood-brain barrier cellular injury or infection (Abbott et al. 2010; Chodobski et al. 2011; Wolburg et al. 2009). In this study, the animals were followed for only 24 h; a longer survival time is needed to establish the profile of astroglial activation.

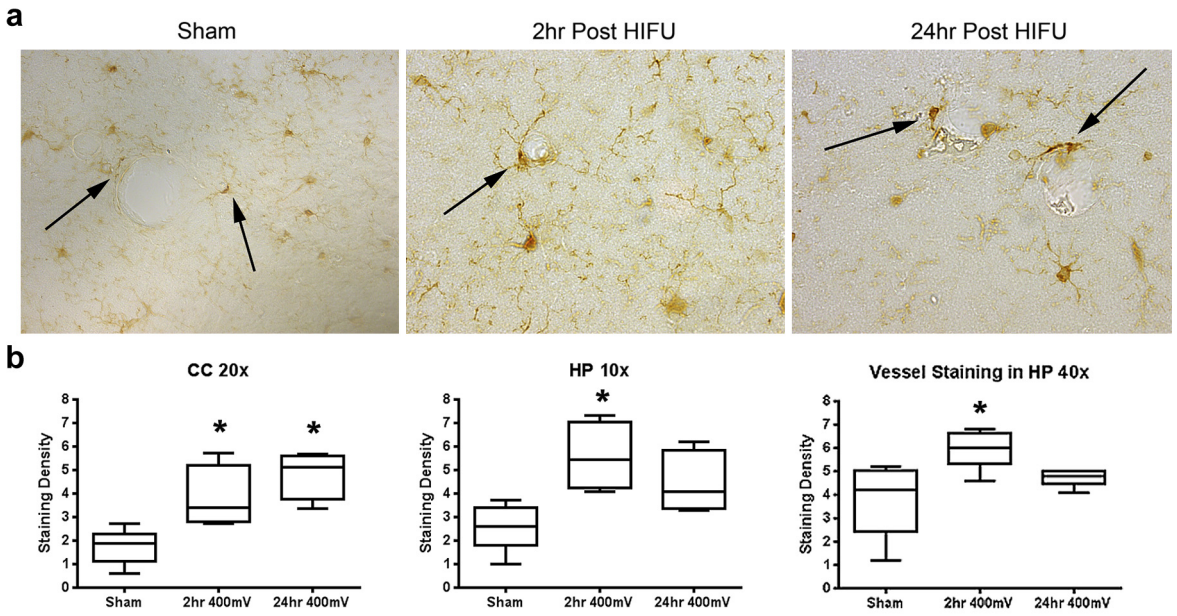

Fig. 8. Staining for Iba1 after exposure to HIFU. The images (a) illustrate Iba1 staining of microglia and perivascular cells (a, *arrows*) in the hippocampus after sham treatment (no exposure to a HIFU wave) and 2 and 24 h after HIFU exposure. There was a very modest increase in the number of labeled cell profiles, but a more evident increase in the staining intensity. The graphs (b) illustrate the changes in staining density 2 and 24 h after HIFU exposure. Analysis of variance revealed significant changes in staining density for Iba1 (indicated by asterisks) after HIFU exposure in the CC (2-h $p < 0.007$ and 24-h $p = 0.001$ vs. sham group) and HP (2-h $p = 0.005$ vs. sham group). A measure of immunostaining for Iba1 near blood vessels in the HP indicated staining density for Iba1 was elevated 2 h after HIFU exposure ($p = 0.016$ vs. sham group). Iba1 = ionized calcium-binding adaptor molecule 1, HIFU = high-intensity focused ultrasound, CC = corpus callosum, HP = hippocampus.

Microglial activation is considered to have a significant role in neuro-inflammatory-related secondary damage from brain injury (Loane and Byrnes 2010), as well as a potential beneficial function (Aguzzi et al. 2013), and that activation may be a hallmark of the long-lasting effects from TBI and neural degeneration (Block et al. 2007; Smith 2013; Taber et al. 2006). Iba1 (also called allograft inflammatory factor 1) has been used as a cell marker for resident microglia and perivascular cells (Ito et al. 1998). Elevation of Iba1 staining in microglia in the present study suggests mild stimulation results in at least transient alteration. Together, the IgG, GFAP and Iba1 results indicate a perturbation of the blood-brain barrier with a neuro-immune response. Because of the short time span of the study, it is not possible to establish if the neuro-immune response is a transient response, which could resolve quickly because of a lack of sustained cell damage, or if the low-level neuro-immune response persists.

Although these effects are indicative of brain injury, they are less severe than those that have been observed in shock tubes. Reneer et al. (2011), for example, observed hematomas in the brains of rats exposed to shock tube overpressures of about 100 kPa. Moochhala et al. (2004) detonated explosives in the vicinity of rats and detected degenerating cortical neurons, when the blast overpressure was about 20 kPa. By comparison, the RMS pressures associated with the bio-effects documented in this study were on the order of 1000 kPa (Fig. 4, *middle*). The difference in biological effects is likely related to the presence of both positive (compressive) and negative (tensile) pressures in the HIFU-simulated overpressure, whereas the blast overpressure is completely positive.

A more relevant predictor of the effects generated by the HIFU wave than the RMS pressure or amplitude of the oscillating pressure may be the radiation pressure, in the following sense. The radiation force is the time-averaged force exerted by the ultrasound beam on a liquid or soft tissue medium, arising from absorption of the ultrasound energy by the medium. The radiation force acts in the direction of beam propagation. Because it continually pushes on the absorbing medium, that is, there is no oscillation in the force, it may more closely simulate the blast overpressure. Mathematically, the radiation pressure is given by Wahab et al. (2012) as

$$p_{\mathrm{rad}} = \frac{2\alpha\delta}{\rho_0 c_0^2} p_{\mathrm{rms}}^2 \tag{5}$$

The quantities, α, ρ_0, c_0 and p_{rms} were defined in the previous section, and δ represents the ultrasound beam width. Using soft tissue values given above, a value of 2.5 mm for the ultrasound beam width in the mouse and 3 MPa as the maximum RMS pressure in the mouse skull (Fig. 3b), the radiation pressure would vary over the simulated overpressure between 0 and 200 Pa (0.2 kPa). This is considerably smaller than the overpressure measured in shock tubes (Reneer et al. 2011) and actual detonations (Moochhala et al. 2004).

To the extent that the brain tissue responds to the radiation pressure and not the oscillatory pressure for a HIFU pulse train, the lower level of damage observed in the present study is consistent with that observed with shock tubes and detonations.

For further comparison of the HIFU blast-overpressure model with other methods, waveforms for different blast simulators are plotted in Figure 9. The durations of the overpressures are between 2.0 and 4.0 ms. Because of the large variation in pressure levels, a decibel scale (relative to 1.0 MPa) is used. Both the RMS pressure and radiation pressure are illustrated for the HIFU model. Also illustrated are waveforms for explosive detonations measured by Moochhala et al. (maximum pressure = 100 psi = 690 kPa, from Moochhala et al. [2004:Fig. 2]) and for shock-tube measurements made by Chavko et al. (maximum pressure = 40 kPa, from Chavko et al. [2007:Fig. 5]). All curves begin with a rapid rise, though the exact rise time is difficult to discern from data digitized from published detonation and shock-tube studies, and no quantitative conclusions regarding precise rise time should be drawn. The approximately linear behavior between times of about 0.3 to 1.5 ms that all the curves exhibit on the decibel scale is reflective of an exponentially decaying overpressure. After approximately 1.5 ms, the HIFU curves and the detonation pressures of Moochhala et al. start to exhibit a sharper decrease. (The shock-tube measurements of Chavko et al. exhibit this behavior slightly later, around 3.0 ms.) The waveforms in Figure 9 are similar in shape, though they are different in magnitude and produce different levels of brain injury. To preserve the correct rank of the curves, that is, higher pressures produce larger effects, we work with the radiation pressure rather than the RMS pressure. As discussed above, this is sensible on a physical basis, as the force due to the radiation pressure is unidirectional for the duration of the overpressure, similar to a blast wave. But unlike a blast wave, the partially counteracting positive and negative pressure oscillations in a HIFU-simulated overpressure contribute collaboratively to the RMS pressure (as only the pressure magnitude is relevant), resulting in relatively high RMS pressures being associated with relatively minor injury. Another way of saying this is that the RMS pressure is really a measure of total acoustic energy, which is not the best indicator of level or type of mTBI.

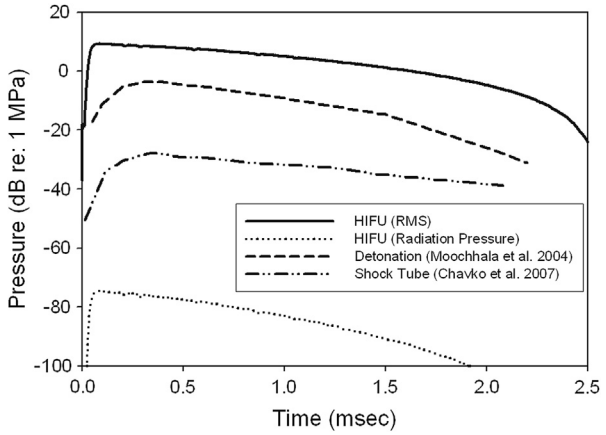

Fig. 9. Time profiles of high-intensity focused ultrasound (HIFU), detonation blast and shock tube overpressure waves. For comparison, pressure is expressed in decibels and suggests similar overpressure waveforms are observed in each model. The root-mean-square (RMS) pressure of the HIFU profile is greater than after detonation or shock tube emission. However, radiation pressure from HIFU is considerably less, consistent with levels of brain injury observed.

Calibration of the HIFU blast model, that is, identifying which bio-effects occur at what pressure levels relative to detonation and shock-tube models, requires bio-effect data for shock-tube and detonation studies performed at overpressures lower in magnitude than those in Figure 9 and for HIFU studies performed at radiation pressures higher than those in Figure 9. Säljö et al. (2009) found evidence of mTBI produced by shock-tube pressures as low as 10 kPa (–40 dB re: 1 MPa [Säljö et al. 2009]). This evidence was obtained primarily from behavioral studies. Similar studies are planned for HIFU-based mTBIs. To generate more intense radiation pressures with HIFU, a higher-gain (more focused) transducer will be used. Care must be taken that the peak negative pressure (discussed above) does not exceed the cavitation threshold. Fortunately, because of non-linear propagation effects occurring in the 1.5-MHz carrier wave of the amplitude-modulated HIFU pulse, significant changes in positive pressure are accompanied by only minor changes in negative pressure (see Fig. 2, *bottom traces*).

In addition to pressure level, exposure duration likely plays a role in blood-brain barrier disruption and other manifestations of TBI. In their study of blood-brain barrier disruption in rats caused by exposure to 2-MHz, continuous-wave HIFU of intensity 485 W/cm^2, Mesiwala et al. (2002) observed blood-brain barrier opening 64% of the time. Sixty percent of these openings occurred without parenchymal damage; the remainder

manifested injury such as hemorrhage. The radiation pressure associated with the HIFU beam of Mesiwala et al. is approximately 130 Pa, slightly less than the maximum radiation pressure during our simulated overpressure. Mesiwala et al., however, used a much longer exposure, 0.2 s. For a future comparison with the research of Mesiwala et al, the duration of the HIFU-simulated blast overpressure can be easily lengthened by adjusting the settings of the second function generator shown in Figure 2. Comparison with the work of Säljö et al. cited above would also require increasing the pulse train length to 6 ms. For the present, it can be said that the observations of Mesiwala et al. and the present study are consistent with the following statements: (i) Blood-brain barrier disruption can be induced with HIFU wave trains having radiation pressure values on the order of 100 Pa, for exposures as short as 1 ms. (ii) Longer exposure times can begin to produce parenchymal damage.

Although the HIFU model has been able to produce manifestations of mTBI known to occur during blasts, such as blood-brain barrier disruption and intensified immune response, it must also be recognized that differences between the HIFU model and actual blasts will likely exist. Bio-effects caused by shearing of tissue within the brain, for example, could be different for HIFU pulse trains and actual blasts. Because blast waves are essentially uniform over the entire external surface of the skull, shearing occurs as a result of tissue property differences within the skull. Shearing caused by tissue property differences will also occur with HIFU pulse trains, particularly if the scale over which the variations occur is smaller than the beam width. (The HIFU beam width is characterized in Fig. 4.) However, shearing caused by HIFU can also occur in homogeneous tissue, in the manner in which shear waves are created in elastography (Parker et al. 2011), as a result of the variation in the pressure field across the beam. This effect is very localized within the brain. If duplicating shearing effects is critical, differences between HIFU and actual blasts can be minimized by using wider HIFU beams. Some of the differences between HIFU-simulated overpressures and blast overpressures will emerge only after both models are used extensively under similar conditions. This includes evaluating both methods based on comprehensive behavioral tests on cohorts of animals exposed to both blast types. In cases where similar bio-effects are produced by the HIFU model and actual blasts, the convenience, controllability and tolerability of HIFU make it an attractive alternative.

CONCLUSIONS

High-intensity focused ultrasound allows for the generation of simulated blast overpressures in a controllable, tolerable and inexpensive manner. Exposure of mice to HIFU-simulated overpressures produced manifestations of mild traumatic brain injury, such as blood brain-barrier disruption, antibody accumulation in vascular walls and activation of astrocytes and microglia. Evidence of moderate to severe brain injury, such as hemorrhage and neuron cell death, was not observed. Further work is needed to validate the methodology and related changes using animals that have sustained mild injuries in blast tubes and using actual injuries seen in victims who sustain blast-induced traumatic brain injury. Although HIFU is not intended to completely replace actual detonations or shock tubes, it may serve as a valuable surrogate for the simulation of some of the phenomenology associated with human blast-induced mild traumatic brain injury.

Acknowledgments—This work was supported by U.S. Army Medical Research and Materiel Command Grant W81 XWH-09-2-0147 and Translational Research Grant Opportunities of the Blast Lethality Injury and Research Program Grant 600-070-00000-00-106108 to J.T.M., and Project G183 YL from The Center for Neuroscience and Regenerative Medicine to C.M.—The experiments were conducted according to the principles set forth in the *Guide for Care and Use of Laboratory Animals*, ILAR, National Research Council, DHEW Publication (NIH) 73-23. The opinions, interpretations, conclusions and recommendations are those of the authors and are not necessarily endorsed by the U.S. Army, Department of Defense, U.S. government or Uniformed Services University of the Health Sciences. The use of trade names does not constitute an official endorsement or approval of the use of such reagents or commercial hardware or software. This document may not be cited for purposes of advertisement.

REFERENCES

Abbott NJ, Patabendige AA, Dolman DE, Yusof SR, Begley DJ. Structure and function of the blood-brain barrier. Neurobiol Dis 2010;37:13–25.

Abbott NJ, Rönnbäck L, Hansson E. Astrocyte-endothelial interactions at the blood-brain barrier. Nat Rev Neurosci 2006;7:41–53.

Aguzzi A, Barres BA, Bennett ML. Microglia: Scapegoat, saboteur, or something else? Science 2013;339:156–161.

Aschkenasy-Steuer G, Shamir M, Rivkind A, Mosheiff R, Shushan Y, Rosenthal G, Mintz Y, Weissman C, Sprung CL, Weiss YG. Clinical review: The Israeli experience: Conventional terrorism and critical care. Crit Care 2005;9:490–499.

Bass CR, Panzer MB, Rafaels KA, Wood G, Shridharani J, Capehart B. Brain injuries from blast. Ann Biomed Eng 2011;40:185–202.

Bauman RA, Ling G, Tong L, Januszkiewicz A, Agoston D, Delanerolle N, Kim Y, Ritzel D, Bell R, Ecklund J, Armonda R, Bandak F, Parks S. An introductory characterization of a combat-casualty-care relevant swine model of closed head injury resulting from exposure to explosive blast. J Neurotrauma 2009;26:841–860.

Bazarian JJ, Cernak I, Noble-Haeusslein L, Potolicchio S, Temkin N. Long-term neurologic outcomes after traumatic brain injury. J Head Trauma Rehabil 2009;24:439–451.

Block ML, Zecca L, Hong JS. Microglia-mediated neurotoxicity: Uncovering the molecular mechanisms. Nat Rev Neurosci 2007;8:57–69.

Brown AW, Moessner AM, Mandrekar J, Diehl NN, Leibson CL, Malec JF. A survey of very-long-term outcomes after traumatic brain injury among members of a population-based incident cohort. J Neurotrauma 2011;28:167–176.

Cernak I, Savic J, Ignjatovic D, Jevtic M. Blast injury from explosive munitions. J Trauma 1999;47:96–103.

Chavko M, Koller WA, Prusaczyk WK, McCarron RM. Measurement of blast wave by a miniature fiber optic pressure transducer in the rat brain. J Neurosci Methods 2007;159:277–281.
Chavko M, Prusaczyk WK, McCarron RM. Protection against blast-induced mortality in rats by hemin. J Trauma 2008;65:1140–1145.
Chen Y, Huang W. Non-impact, blast-induced mild TBI and PTSD: concepts and caveats. Brain Inj 2011;25:641–650.
Chodobski A, Zink BJ, Szmydynger-Chodobska J. Blood-brain barrier pathophysiology in traumatic brain injury. Transl Stroke Res 2011;2:492–516.
Collins TJ. ImageJ for microscopy. BioTechniques 2007;43:25–30.
Desmoulin GT, Dionne JP. Blast-induced neurotrauma: Surrogate use, loading mechanisms, and cellular responses. J Trauma 2009;67: 1113–1122.
DuBose JJ, Barmparas G, Inaba K, Stein DM, Scalea T, Cancio LC, Cole J, Eastridge B, Blackbourne L. Isolated severe traumatic brain injuries sustained during combat operations: Demographics, mortality outcomes, and lessons to be learned from contrasts to civilian counterparts. J Trauma 2011;70:11–16.
Duck FA. Physical properties of tissues: A comprehensive reference notebook. San Diego: Academic Press; 1990.
Elder GA, Cristian A. Blast-related mild traumatic brain injury: Mechanisms of injury and impact on clinical care. Mt Sinai J Med 2009; 76:111–118.
Fry FJ, Sanghvi NT, Foster RS, Bihrle R, Hennige C. Ultrasound and microbubbles: Their generation, detection and potential utilization in tissue and organ therapy—Experimental. Ultrasound Med Biol 1995;21:1227–1237.
Gateau J, Aubry JF, Chauvet D, Boch AL, Fink M, Tanter M. *In vivo* bubble nucleation probability in sheep brain tissue. Phys Med Biol 2011;56:7001–7015.
Gavrilov LR, Tsirulnikov EM, Davies IA. Application of focused ultrasound for the stimulation of neural structures. Ultrasound Med Biol 1996;22:179–192.
Gorbunov NK, Asher LV, Elsayed NM, Atkins JL. Inflammatory response in primary blast injury. In: Elsayed NM, Atkins JL, (eds). Explosion and blast-related injuries. Burlington, MA: Elsevier Academic Press; 2008. p. 298–303.
Hawkins BT, Davis TP. The blood-brain barrier/neurovascular unit in health and disease. Pharmacol Rev 2005;57:173–185.
International Commission on Radiation Units and Measurements (ICRU). Tissues substitutes, phantoms and computation modeling in medical ultrasound. ICRU Report 61. Bethesda, MD; 1998.
Ito D, Imai Y, Ohsawa K, Nakajima K, Fukuuchi Y, Kohsaka S. Microglia-specific localisation of a novel calcium binding protein, Iba1. Brain Res Mol Brain Res 1998;57:1–9.
Kulik L, Fleming SD, Moratz C, Reuter JW, Novikov A, Chen K, Andrews KA, Markaryan A, Quigg RJ, Silverman GJ, Tsokos GC, Holers VM. Pathogenic natural antibodies recognizing annexin IV are required to develop intestinal ischemia-reperfusion injury. J Immunol 2009;182:5363–5373.
Loane DJ, Byrnes KR. Role of microglia in neurotrauma. Neurotherapeutics 2010;7:366–377.
Long JB, Bentley TL, Wessner KA, Cerone C, Sweeney S, Bauman RA. Blast overpressure in rats: Recreating a battlefield injury in the laboratory. J Neurotrauma 2009;26:827–840.
Mesiwala AH, Farrell L, Wenzel HJ, Silbergeld DL, Crum LA, Winn HR, Mourad PD. High-intensity focused ultrasound selectively disrupts the blood-brain barrier *in vivo*. Ultrasound Med Biol 2002;28:389–400.
Min BK, Bystritsky A, Jung KI, Fischer K, Zhang Y, Maeng LS, Park SI, Chung YA, Jolesz FA, Yoo SS. Focused ultrasound-mediated suppression of chemically-induced acute epileptic EEG activity. BMC Neurosci 2011;12:23.
Moochhala SM, Md S, Lu J, Teng CH, Greengrass C. Neuroprotective role of aminoguanidine in behavioral changes after blast injury. J Trauma 2004;56:393–403.
Myer DJ, Gurkoff GG, Lee SM, Hovda DA, Sofroniew MV. Essential protective roles of reactive astrocytes in traumatic brain injury. Brain 2006;129:2761–2772.
Myers MR, Soneson JE. Temperature modes for nonlinear Gaussian beams. J Acoust Soc Am 2009;126:425–433.
Nyborg WL. Solutions of the bio-heat transfer equation. Phys Med Biol 1988;33:785–792.
Park J, Zhang Y, Vykhodtseva N, Jolesz FA, McDannold NJ. The kinetics of blood brain barrier permeability and targeted doxorubicin delivery into brain induced by focused ultrasound. J Control Release 2012;162:134–142.
Parker KJ, Doyley MM, Rubens DJ. Imaging the elastic properties of tissue: The 20 year perspective. Phys Med Biol 2011;56:R1–R29.
Rao LV, Pendurthi UR. Regulation of tissue factor coagulant activity on cell surfaces. J Thromb Thrombolysis 2012;10:2242–2253.
Reneer DV, Hisel RD, Hoffman JM, Kryscio RJ, Lusk BT, Geddes JW. A multi-mode shock tube for investigation of blast-induced traumatic brain injury. J Neurotrauma 2011;28:95–104.
Risling M, Davidsson J. Experimental animal models for studies on the mechanisms of blast-induced neurotrauma. Front Neurol 2012;3:30.
Rosenberg GA. Neurological diseases in relation to the blood-brain barrier. J Cereb Blood Flow Metab 2012;32:1139–1151.
Säljö A, Svensson B, Mayorga M, Hamberger A, Bolouri H. Low levels of blast raises intracranial pressure and impairs cognitive function in rats. J Neurotrauma 2009;26:1345–1352.
Samiotaki G, Vlachos F, Tung YS, Konofagou EE. A quantitative pressure and microbubble-size dependence study of focused ultrasound-induced blood-brain barrier opening reversibility in vivo using MRI. Magn Reson Med 2012;67:769–777.
Sayer NA, Chiros CE, Sigford B, Scott S, Clothier B, Pickett T, Lew HL. Characteristics and rehabilitation outcomes among patients with blast and other injuries sustained during the Global War on Terror. Arch Phys Med Rehabil 2008;89:163–170.
Schmued LC, Hopkins KJ, Fluoro-Jade B. A high affinity fluorescent marker for the localization of neuronal degeneration. Brain Res 2000;874:123–130.
Silver JM, Mc Allister TW, Arciniegas DB. Depression and cognitive complaints following mild traumatic brain injury. Am J Psychiatry 2009;166:653–661.
Smith C. Review: The long-term consequences of microglial activation following acute traumatic brain injury. Neuropathol Appl Neurobiol 2013;39:35–44.
Sundaramurthy A, Alai A, Ganpule S, Holmberg A, Plougonven E, Chandra N. Blast-induced biomechanical loading of the rat: An experimental and anatomically accurate computational blast injury model. J Neurotrauma 2012;29:2352–2364.
Svetlov SI, Prima V, Kirk DR, Gutierrez H, Curley KC, Hayes RL, Wang KK. Morphologic and biochemical characterization of brain injury in a model of controlled blast overpressure exposure. J Trauma 2010;69:795–804.
Taber KH, Warden DL, Hurley RA. Blast-related traumatic brain injury: What is known? J Neuropsychiatry Clin Neurosci 2006; 18:141–145.
Tanielian T, Jaycox LH. Invisible wounds of war: psychological and cognitive injuries, their consequences, and services to assist recovery. Santa Monica, CA: RAND Corporation Monograph Series; 2008.
Ter Haar G. Therapeutic applications of ultrasound. Prog Biophys Mol Biol 2007;93:111–129.
Tufail Y, Matyushov A, Baldwin N, Tauchmann ML, Georges J, Yoshihiro A, Tillery SI, Tyler WJ. Transcranial pulsed ultrasound stimulates intact brain circuits. Neuron 2010;66:681–694.
Tyler WJ, Tufail Y, Finsterwald M, Tauchmann ML, Olson EJ, Majestic C. Remote excitation of neuronal circuits using low-intensity, low-frequency ultrasound. PLoS ONE 2008;3:e3511.
Wahab RA, Choi M, Liu Y, Krauthamer V, Zderic V, Myers MR. Mechanical bioeffects of pulsed high intensity focused ultrasound on a simple neural model. Med Phys 2012;39:4274–4283.
Wojcik BE, Stein CR, Bagg K, Humphrey RJ, Orosco J. Traumatic brain injury hospitalizations of U.S. army soldiers deployed to Afghanistan and Iraq. Am J Prev Med 2010;38:S108–S116.
Wolburg H, Noell S, Mack A, Wolburg-Buchholz K, Fallier-Becker P. Brain endothelial cells and the glio-vascular complex. Cell Tissue Res 2009;335:75–96.